

Supernova Interaction with a Circumstellar Medium

Roger A. Chevalier¹ and Claes Fransson²

¹ Department of Astronomy, University of Virginia, P.O. Box 3818,
Charlottesville, VA 22903, USA

² Stockholm Observatory, Department of Astronomy, SCFAB,
SE-106 91 Stockholm, Sweden

Abstract. The explosion of a core collapse supernova drives a powerful shock front into the wind from the progenitor star. A layer of shocked circumstellar gas and ejecta develops that is subject to hydrodynamic instabilities. The hot gas can be observed directly by its X-ray emission, some of which is absorbed and re-radiated at lower frequencies by the ejecta and the circumstellar gas. Synchrotron radiation from relativistic electrons accelerated at the shock fronts provides information on the mass loss density if free-free absorption dominates at early times or the size of the emitting region if synchrotron self-absorption dominates. Analysis of the interaction leads to information on the density and structure of the ejecta and the circumstellar medium, and the abundances in these media. The emphasis here is on the physical processes related to the interaction.

1 Introduction

The collision of supernova ejecta with dense surrounding gas can generate high pressure regions comparable to those found in the emission regions of active galactic nuclei. The shock wave interactions are analogous to those occurring in γ -ray burst afterglows, although the supernova case involves nonrelativistic velocities. Multiwavelength observations, when combined with models for the emission, give detailed information on the outer supernova structure and the structure of the surrounding mass loss region. The stellar mass loss history leading up to the supernova explosion can be deduced from the surrounding structure.

The study of circumstellar interaction around supernovae has benefitted from several developments in the observational investigations of supernovae. One is the ability to observe supernovae in wavelength regions other than optical. Radio, X-ray, infrared, and ultraviolet observations have all been crucial for revealing various aspects of circumstellar interaction. Another is the ability to follow the optical emission from supernovae to late times with the new generation of large telescopes. The emission from circumstellar interaction typically has a lower decay rate than does the inner emission from gas heated by the initial explosion and by radioactivity, so that it eventually comes to dominate the emission. Finally, the interest in supernovae generated by SN 1987A and other events has increased the rate of supernova discovery, including events which show signs of circumstellar interaction from a young age.

Many of the observational manifestations of circumstellar interaction are treated in other chapters of this volume. The emphasis here is on providing the theoretical basis to model the observed phenomena. The structure of the freely expanding supernova ejecta and of the surrounding medium provide the initial conditions for the interaction and are discussed in the first two sections. Section 4 deals with the hydrodynamics of the interaction and section 5 treats the emission from hot gas. The effects of supernova radiation on the circumstellar gas are discussed in section 6 and relativistic particles in section 7. The discussion and conclusions are in section 8.

2 Ejecta Structure

The density structure of a supernova is set up during the first days after the explosion. Over this timescale, the pressure forces resulting from the initial explosion, and some later power input from radioactivity, become too small to change the supernova density structure. The velocity profile tends toward that expected for free expansion, $v = r/t$, and the density of a gas element drops as t^{-3} . The pressure drops to a sufficiently low value that it is not a factor in considering shock waves propagating in the ejecta as a result of later interaction.

The density structure of the ejecta is a more complex problem. For core collapse supernovae, where all the explosion energy is generated at the center of the star, the explosion physics lead to an outer, steep power law density profile along with an inner region with a relatively flat profile [17,62]. The outer profile is produced by the acceleration of the supernova shock front through the outer stellar layers with a rapidly decreasing density. This part of the shock propagation does not depend on the behavior in the lower layers and the limiting structure is described by a self-similar solution. The structure depends on the initial structure of the star and thus depends on whether the progenitor star has a radiative or a convective envelope [62]. In the radiative case, which applies to Wolf-Rayet stars and to progenitors like that of SN 1987A, the limiting profile is $\rho \propto r^{-10.2}$. In the convective case, which applies to red supergiant progenitors, the limiting profile is $\rho \propto r^{-11.7}$. These are the limiting profiles and the density profile over a considerable part of the supernova might be described by a somewhat flatter profile. Numerical calculations of the explosion of SN 1987A have indicated $\rho \propto r^{-(8-9)}$ in the outer parts of the supernova [1].

The calculations of the density profile assume an adiabatic flow. As the shock wave approaches the surface of the star, radiative diffusion becomes a factor and the shock acceleration stops. In the case of SN 1987A, theory as well as observations suggest that diffusion is not important until a velocity of $\sim 30,000 \text{ km s}^{-1}$ is reached [33]. A comparable limit applies to the relatively compact progenitors of the Wolf-Rayet star explosions [62]. In the case of red supergiant progenitors, which is the case applicable to most Type II supernovae, a lower velocity limit is expected. At the point in the shock evolution where radiative diffusion becomes important, the loss of the radiative energy can lead to a large compression of the gas, to the point where the thermal pressure becomes important [7]. There is the

possibility of a dense shell at the maximum velocity generated by the supernova. The shell may be broken up by Rayleigh-Taylor instabilities [35] and the final outcome of these processes is not known.

The overall result of these considerations is that the outer part of a core collapse supernova can be approximated by a steep power law density profile, or $\rho_{\text{ej}} \propto r^{-n}$ where n is a constant. After the first few days the outer parts of the ejecta expand with constant velocity, $V(m) \propto r$ for each mass element, m , so that $r(m) = V(m)t$ and $\rho(m) = \rho_o(m)(t_o/t)^3$. Therefore

$$\rho_{\text{ej}} = \rho_o(t/t_o)^{-3}(V_o t/r)^n. \quad (1)$$

This expression takes into account the free expansion of the gas.

Type Ia supernovae, which are believed to be the thermonuclear explosions of white dwarfs, are different because the supernova energy is not all centrally generated. A burning front spreads through the star and the energy released in this way gives rise to an explosion. The results of a number of explosion simulations show that the post-explosion density profile can be approximated by an exponential in velocity [27].

3 Stellar Mass Loss

Type II supernovae, with H lines in their spectra, are thought to be the explosions of massive stars that have reached the ends of their lives with their H envelopes. In most cases, the stars explode as red supergiants, which are known to have slow, dense winds. Typical parameters are a mass loss rate of $\dot{M} = 10^{-6} - 10^{-4} M_{\odot} \text{ yr}^{-1}$ and a wind velocity $u_w = 5 - 25 \text{ km s}^{-1}$. If the mass loss parameters stay approximately constant leading up to the explosion, the circumstellar density is given by

$$\rho_{\text{cs}} = \dot{M}/(4\pi u_w r^2). \quad (2)$$

In the late stellar evolutionary phases, the evolution of the stellar core occurs on a rapid timescale, but the stellar envelope has a relatively long dynamical time, which can stabilize the mass loss properties.

The mechanisms by which mass is lost in the red supergiant phase are poorly understood, but some insight into the wind properties can be gained by considering observations of the winds. VY CMa, thought to have a zero-age main sequence mass of $30 - 40 M_{\odot}$ [81], a mass loss rate $\sim 3 \times 10^{-4} M_{\odot} \text{ yr}^{-1}$, and $u_w \approx 39 \text{ km s}^{-1}$ [25,69], is an especially well-observed case. *HST* imaging shows that the density profile is approximately r^{-2} over the radius range $3 \times 10^{16} - 1.4 \times 10^{17} \text{ cm}$ but that there is considerable structure superposed on this profile, including knots and filaments [69]. Observations of masers imply the presence of clumps with densities up to $\sim 5 \times 10^9 \text{ cm}^{-3}$ and suggest the presence of an expanding disk seen at an oblique angle [67]. VY CMa is an extreme mass loss object, but there is evidence for irregular mass loss in α Orionis and other red supergiants [75,76]. Among lower mass stars, the bipolar structure of

planetary nebulae has been widely attributed to a high equatorial density in the red giant wind. In one case where we can observe the circumstellar surroundings of a supernova, SN 1987A, an axisymmetric structure similar to that found in planetary nebulae has been observed [6].

Some massive stars, either through individual mass loss or through binary interaction, lose their H envelopes entirely and become Wolf-Rayet stars. Their ultimate explosions are thought to be observed as Type Ib and Ic supernovae. The progenitor stars are more compact in this case and have faster winds, with $u_w = 1,000 - 2,500 \text{ km s}^{-1}$ and $\dot{M} = 10^{-6} - 10^{-4} M_\odot \text{ yr}^{-1}$ [80]. The fast wind can create a bubble in the surrounding medium, which is typically the slow wind from a previous evolutionary phase, and the resulting shells have been observed around a number of Wolf-Rayet stars [45]. Their typical radii are a few pc.

The progenitors of Type Ia supernovae are not known, so that observations of circumstellar interaction as well as other signatures of the companion star potentially contain important clues on the progenitor question [5,24,59]. In models where a white dwarf accretes mass from a companion star, the wind from the companion can provide a relatively dense circumstellar medium. In the case of a double degenerate progenitor, there may be a disk around the coalesced object, but the interaction is with the interstellar medium on larger scales. There have been no detections of circumstellar interaction around Type Ia supernovae, so we do not discuss them further in this review, although the physical processes described here should apply if any surrounding wind is present.

4 Hydrodynamics

When the radiation dominated shock front in a supernova nears the stellar surface, a radiative precursor to the shock forms when the radiative diffusion time is comparable to the propagation time. There is radiative acceleration of the gas and the shock disappears when optical depth \sim unity is reached [33]. The fact that the velocity decreases with radius implies that the shock will re-form as a viscous shock in the circumstellar wind. This occurs when the supernova has approximately doubled in radius.

The interaction of the ejecta, expanding with velocity $\gtrsim 10^4 \text{ km s}^{-1}$, and the nearly stationary circumstellar medium results in a reverse shock wave propagating inwards (in mass), and an outgoing circumstellar shock. The density in the circumstellar gas is given by equation (2). As discussed above, hydrodynamical calculations show that to a good approximation the ejecta density can be described by equation (1). A useful similarity solution for the interaction can then be found [8,9,64]. Here we sketch a simple derivation. More details can be found in these papers, as well as in the review [11].

Assume that the shocked gas can be treated as a thin shell with mass M_s , velocity V_s , and radius R_s . Balancing the ram pressure from the circumstellar gas and the impacting ejecta, the momentum equation for the shocked shell of

circumstellar gas and ejecta is

$$M_s \frac{dV_s}{dt} = 4\pi R_s^2 [\rho_{\text{ej}}(V - V_s)^2 - \rho_{\text{cs}} V_s^2]. \quad (3)$$

Here, M_s is the sum of the mass of the shocked ejecta and circumstellar gas. The swept up mass behind the circumstellar shock is $M_{\text{cs}} = \dot{M} R_s / u_w$, and that behind the reverse shock $M_{\text{rev}} = 4\pi t_o^3 V_o^n (t/R_s)^{n-3} / (n-3)$, assuming that $R_s \gg R_p$, the radius of the progenitor. With $V = R_s/t$ we obtain

$$\begin{aligned} & \left[\frac{\dot{M}}{u_w} R_s + \frac{4\pi \rho_o t_o^3 V_o^n t^{n-3}}{(n-3) R_s^{n-3}} \right] \frac{d^2 R_s}{dt^2} = \\ & 4\pi R_s^2 \left[\frac{\rho_o t_o^3 V_o^n t^{n-3}}{R_s^n} \left(\frac{R_s}{t} - \frac{dR_s}{dt} \right)^2 - \frac{\dot{M}}{4\pi u_w R_s^2} \left(\frac{dR_s}{dt} \right)^2 \right]. \end{aligned} \quad (4)$$

This equation has the power law solution

$$R_s(t) = \left[\frac{8\pi \rho_o t_o^3 V_o^n u_w}{(n-4)(n-3) \dot{M}} \right]^{1/(n-2)} t^{(n-3)/(n-2)}. \quad (5)$$

The form of this similarity solution can be written down directly by dimensional analysis from the only two independent quantities available, $\rho_o t_o^3 V_o^n$ and \dot{M}/u_w . The solution applies after a few expansion times, when the initial radius has been ‘forgotten.’ The requirement of a finite energy in the flow implies $n > 5$. More accurate similarity solutions, taking the structure within the shell into account, are given in [8,64]. In general, these solutions differ by less than $\sim 30\%$ from the thin shell approximation.

The maximum ejecta velocity close to the reverse shock depends on time as $V = R_s/t \propto t^{-1/(n-2)}$. The velocity of the circumstellar shock, dR_s/dt , in terms of V is $V_s = V(n-3)/(n-2)$ and the reverse shock velocity, $V_{\text{rev}} = V - V_s = V/(n-2)$. Assuming cosmic abundances and equipartition between ions and electrons, the temperature of the shocked circumstellar gas is

$$T_{\text{cs}} = 1.36 \times 10^9 \left(\frac{n-3}{n-2} \right)^2 \left(\frac{V}{10^4 \text{ km s}^{-1}} \right)^2 \text{ K} \quad (6)$$

and at the reverse shock

$$T_{\text{rev}} = \frac{T_{\text{cs}}}{(n-3)^2}. \quad (7)$$

The time scale for equipartition between electrons and ions is

$$t_{\text{eq}} \approx 2.5 \times 10^7 \left(\frac{T_e}{10^9 \text{ K}} \right)^{1.5} \left(\frac{n_e}{10^7 \text{ cm}^{-3}} \right)^{-1} \text{ s}. \quad (8)$$

One finds that the reverse shock is marginally in equipartition, unless the temperature is $\gtrsim 5 \times 10^8 \text{ K}$. The ion temperature behind the circumstellar shock is

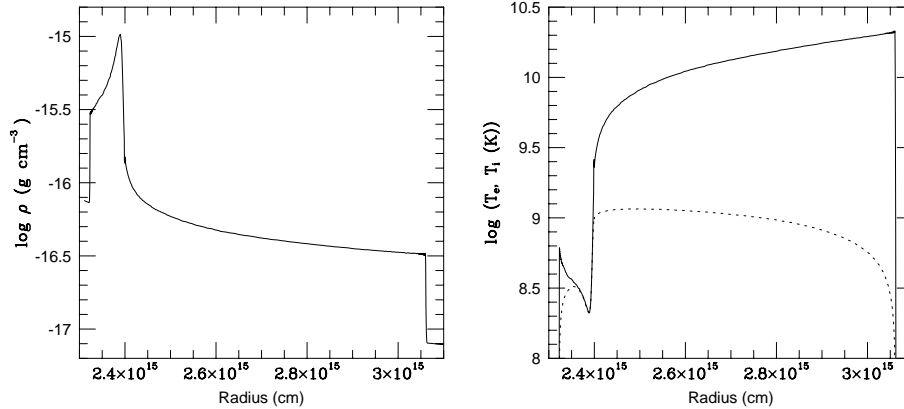


Fig. 1. Density and temperature structure of the reverse and circumstellar shocks for $n = 7$ and a velocity of $2.5 \times 10^4 \text{ km s}^{-1}$ at 10 days. Both shocks are assumed to be adiabatic. Because of the slow Coulomb equipartition the electron temperature (dotted line) is much lower than the ion temperature (solid line) behind the circumstellar shock.

$\gtrsim 6 \times 10^9 \text{ K}$ for $V_4 \gtrsim 1.5$, and the density a factor $\gtrsim 4$ lower than behind the reverse shock. Ion-electron collisions are therefore ineffective, and $T_e \ll T_{\text{ion}}$, unless efficient plasma instabilities heat the electrons collisionlessly (fig. 1).

For typical parameters, the electron temperatures of the two shocks are very different, $\sim (1-3) \times 10^9 \text{ K}$ for the circumstellar shock and $10^7 - 5 \times 10^8 \text{ K}$ for the reverse shock, depending on n . The radiation from the reverse shock is mainly below $\sim 20 \text{ keV}$, while that from the circumstellar shock is above $\sim 50 \text{ keV}$.

The density behind the reverse shock is

$$\rho_{\text{rev}} = \frac{(n-4)(n-3)}{2} \rho_{\text{cs}} \quad (9)$$

and is much higher than behind the circumstellar shock for $n \gtrsim 7$. There is a drop in density across the contact discontinuity, moving from the shocked ejecta to the circumstellar medium (see fig. 1). The fact that low density gas is decelerating higher density gas leads to a Rayleigh-Taylor instability. Chevalier, Blondin & Emmering [18] have calculated the structure using a two-dimensional PPM (piecewise parabolic method) hydrodynamic code. They indeed find that instabilities develop, with dense, shocked ejecta gas penetrating into the hotter, low density shocked circumstellar gas (fig. 2). The instability mainly distorts the contact surface, and does not seriously affect the general dynamics. The calculation assumed that cooling is not important. If the gas at the reverse shock cools efficiently, the extent of the instability is similar, although the Rayleigh-Taylor fingers are narrower [13].

In view of the evidence for dense equatorial winds from red supergiant stars, Blondin, Lundqvist, & Chevalier [4] simulated the interaction of a supernova with such a wind. They found that for relatively small values of the angular density

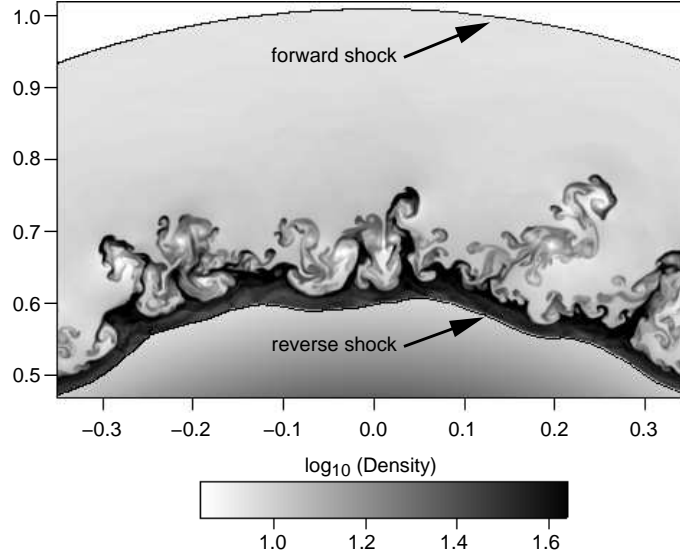


Fig. 2. Two-dimensional calculation of the shock structure for a supernova with $n = 6$ in a stellar wind (courtesy John Blondin).

gradient, the asymmetry in the interaction shell is greater than, but close to, that expected from purely radial motion. If there is an especially low density close to the pole, the flow qualitatively changes and a protrusion emerges along the axis, extending to 2 – 4 times the radius of the main shell. Protrusions have been observed in the probable supernova remnant 41.9+58 in M82, although the nature of the explosion is not clear in this case [63].

In addition to asymmetric winds, there is evidence for supernova shock waves interacting with clumps of gas in the wind, as have been observed in some red supergiant winds (section 3). In some cases the clumps can be observed by their very narrow lines in supernova spectra, as in Type II_n supernovae. The velocity of a shock wave driven into a clump, v_c , can be estimated by approximate pressure balance $v_c \approx v_s(\rho_s/\rho_c)^{1/2}$, where v_s is the shock velocity in the smooth wind with density ρ_s and ρ_c is the clump density. The lower shock velocity and higher density can lead to radiative cooling of the clump shock although the main shock is non-radiative. Optical line emission of intermediate velocity observed in Type II_n (narrow line) supernovae like SN 1978K, SN 1988Z, and SN 1995N can be explained in this way [21,22,44].

The presence of many clumps can affect the hydrodynamics of the interaction. Jun, Jones, & Norman [49] found that propagation in a region with clumps gives rise to widespread turbulence in the shocked region between the forward shock and the reverse shock, whereas the turbulence is confined to a region near the reverse shock for the non-clump case (fig. 2). Their simulations are for interaction

with a constant density medium, but the same probably holds true for interaction with a circumstellar wind.

5 Emission from the hot gas

During the first month, radiation from the supernova photosphere is strong enough for Compton scattering to be the main cooling process for the circumstellar shock. The photospheric photons have energies $\sim 3 kT_{eff} \approx 1 - 10$ eV. The optical depth to electron scattering behind the circumstellar shock is

$$\tau_e = 0.18 \dot{M}_{-5} u_{w1}^{-1} V_4^{-1} t_{\text{days}}^{-1}. \quad (10)$$

A fraction τ_e^N of the photospheric photons will scatter N times in the hot gas. In each scattering the photon increases its energy by a factor $\Delta\nu/\nu \approx 4 kT_e/m_e c^2 \gtrsim 1$. The multiple scattering creates a power law continuum that may reach as far up in energy as the X-ray regime. If relativistic effects can be ignored ($T_e \lesssim 10^9$ K), the spectral index is [37]

$$\alpha = \left\{ \frac{9}{4} - \frac{m_e c^2}{kT_e} \ln \left[\frac{\tau_e}{2} (0.9228 - \ln \tau_e) \right] \right\}^{1/2} - \frac{3}{2}. \quad (11)$$

Typically, $1 \lesssim \alpha \lesssim 3$. This type of emission may have been observed in the ultraviolet emission from SN 1979C [65,37]. For $T_e \gtrsim 10^9$ K relativistic effects become important and considerably increase the cooling [54].

One can estimate the free-free luminosity from the circumstellar and reverse shocks from

$$L_i = 4\pi \int A_{\text{ff}}(T_e) n_e^2 r^2 dr \approx A_{\text{ff}}(T_i) \frac{M_i \rho_i}{(\mu_e m_H)^2}. \quad (12)$$

where the index i refers to quantities connected either with the reverse shock or circumstellar shock. The density behind the circumstellar shock is $\rho_{cs} = 4 \rho_0 = \dot{M}/(\pi u_w R_s^2)$. The swept up mass behind the circumstellar shock is $M_{cs} = \dot{M} R_s / u_w$ and that behind the reverse shock $M_{rev} = (n - 4) M_{cs} / 2$. With $A_{\text{ff}} = 2.4 \times 10^{-27} \bar{g}_{\text{ff}} T_e^{0.5}$, we get

$$L_i \approx 3.0 \times 10^{39} \bar{g}_{\text{ff}} C_n \left(\frac{\dot{M}_{-5}}{u_{w1}} \right)^2 \left(\frac{t}{10 \text{ days}} \right)^{-1} \text{ erg s}^{-1}, \quad (13)$$

where \bar{g}_{ff} is the free-free Gaunt factor, including relativistic effects. For the reverse shock $C_n = (n - 3)(n - 4)^2 / 4(n - 2)$, and for the circumstellar shock $C_n = 1$. This assumes electron-ion equipartition, which is highly questionable for the circumstellar shock (see fig. 1). Because of occultation by the ejecta only half of the above luminosity escapes outward.

At $T_e \lesssim 2 \times 10^7$ K, line emission increases the cooling rate and $\Lambda \approx 3.4 \times 10^{-23} T_{e7}^{-0.67} \text{ erg s}^{-1} \text{ cm}^3$. If the temperature of the reverse shock falls below $\sim 2 \times 10^7$ K, a thermal instability may occur and the gas cools to $\lesssim 10^4$ K, where

photoelectric heating from the shocks balances the cooling. Using $t_{\text{cool}} = 3kT_e/A$, one obtains for the cooling time

$$t_{\text{cool}} = \frac{605}{(n-3)(n-4)(n-2)^{3.34}} \left(\frac{V_{\text{ej}}}{10^4 \text{ km s}^{-1}} \right)^{5.34} \left(\frac{\dot{M}_{-5}}{u_{w1}} \right)^{-1} \left(\frac{t}{\text{days}} \right)^2 \text{ days}, \quad (14)$$

assuming solar abundances [41]. From this expression it is clear that the cooling time is very sensitive to the density gradient, as well as the shock velocity and mass loss rate. SNe with high mass loss rates, like SN 1993J, generally have radiative reverse shocks for $\gtrsim 100$ days, while SNe with lower mass loss rates, like the Type IIP SN 1999em, have adiabatic shocks from early times.

The most important effect of the cooling is that the cool gas may absorb most of the emission from the reverse shock. Therefore, in spite of the higher intrinsic luminosity of the reverse shock, little of this will be directly observable. The column density of the cool gas is given by $N_{\text{cool}} = M_{\text{rev}}/(4\pi R_s^2 m_p)$, or

$$N_{\text{cool}} \approx 1.0 \times 10^{21} (n-4) \left(\frac{\dot{M}_{-5}}{u_{w1}} \right) \left(\frac{V}{10^4 \text{ km s}^{-1}} \right)^{-1} \left(\frac{t}{100 \text{ days}} \right)^{-1} \text{ cm}^{-2}. \quad (15)$$

Because the threshold energy due to photoelectric absorption is related to N_{cool} by $E(\tau = 1) = 1.2(N_{\text{cool}}/10^{22} \text{ cm}^{-2})^{3/8} \text{ keV}$, it is clear that the emission from the reverse shock is strongly affected by the cool shell, and a transition from optically thick to optically thin is expected during the first months, or year. As an illustration, we show in figure 3 the calculated X-ray spectrum at 10 days and at 200 days for SN 1993J [41]. At early epochs the spectrum is dominated by the very hard spectrum from the circumstellar shock, which reaches out to $\gtrsim 100$ keV. At later epochs the soft spectrum from the reverse shock penetrates the cool shell, and the line dominated emission from the cooling gas dominates.

If cooling, the total energy emitted from the reverse shock is

$$\begin{aligned} L_{\text{rev}} &= 4\pi R_s^2 \frac{1}{2} \rho_{\text{ej}} V_{\text{rev}}^3 = \frac{(n-3)(n-4)}{4(n-2)^3} \frac{\dot{M} V^3}{u_w} \\ &= 1.6 \times 10^{41} \frac{(n-3)(n-4)}{(n-2)^3} \dot{M}_{-5} u_{w1}^{-1} V_4^3 \text{ erg s}^{-1}. \end{aligned} \quad (16)$$

For high \dot{M}/u_w the luminosity from the reverse shock may contribute appreciably, or even dominate, the bolometric luminosity.

Because $V \propto t^{-1/(n-2)}$, $L_{\text{rev}} \propto t^{-3/(n-2)}$ in the cooling case. Although the total luminosity is likely to decrease in the cooling case, the increasing transparency of the cool shell, $\tau_{\text{cool}} \propto t^{-1}$, can cause the observed flux in energy bands close to the low energy cutoff, $E(\tau = 1)$, to increase with time, as was seen, e.g., in SN 1993J (figure 3).

Because of the low temperature the spectrum of the reverse shock is dominated by line emission from metals (fig. 3). An important point is that the observed spectrum is formed in gas with widely different temperatures, varying

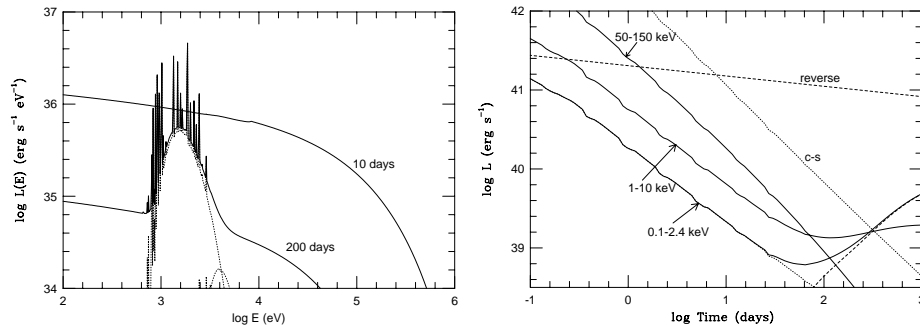


Fig. 3. X-ray spectrum of SN 1993J at 10 days and at 200 days. At 10 days the free-free emission from the outer shock dominates, while at 200 days the cool shell is transparent enough for the line dominated spectrum from the reverse shock to dominate instead. Right: The solid lines give the luminosity in the 0.1-2.4, 1-10, and 50-100 keV bands, corrected for absorption, as a function of time, while the dotted lines give the total emitted luminosity from the reverse and circumstellar shocks [41]

from the reverse shock temperature to $\sim 10^4$ K. A spectral analysis based on a one temperature model can be misleading.

Chugai [19] has proposed that the X-ray emission from the Type II_n SN 1986J is the result of the forward shock front moving into clumps, as opposed to the reverse shock emission. One way to distinguish these cases is by the width of line emission; emission from the reverse shock wave is expected to be broad. It has not yet been possible to carry through with this test [46].

Another way of observing the hot gas is through the emission from collisionally heated dust grains in the gas [30]. Dust formation in the rapidly expanding ejecta is unlikely, so the forward shock front must be considered. Evaporation by the supernova radiation creates a dust-free zone around the supernova (see section 6.3). The time for the supernova shock wave to reach the dust depends on the supernova luminosity and the shock velocity; it is probably at least several years. The infrared luminosity from dust can be up to ~ 100 times the X-ray luminosity of the hot gas for typical parameters, and the dust temperature is a measure of the density of the gas [30]. If the X-ray emission from a supernova like SN 1986J is from circumstellar clumps that are out in the region where dust is present, there is the possibility of a large infrared luminosity.

6 Radiative heating and re-emission

6.1 Soft X-ray burst and circumstellar gas

The earliest form of circumstellar interaction occurs at shock break-out. As the shock approaches the surface, radiation leaks out on a time scale of less than an

hour. The color temperature of the radiation is $\sim (1 - 5) \times 10^5$ K and the energy $\sim (1 - 10) \times 10^{48}$ ergs [51,34,33,62]. This burst of EUV (extreme ultraviolet) and soft X-rays ionizes and heats the circumstellar medium on a time scale of a few hours. In addition, the momentum of the radiation may accelerate the circumstellar gas to a high velocity. Most of the emission at energies $\gtrsim 100$ eV is emitted during the first few hours, and after 24 hours little ionizing energy remains.

The radiative effects of the soft X-ray burst were most clearly seen from the ring of SN 1987A, where a number of narrow emission lines from highly ionized species, like N III-N V, were first seen in the UV [43,72]. Later, a forest of lines came to dominate also the optical spectrum [78]. Imaging with HST (e.g., [47,6]) showed that the lines originated in the now famous circumstellar ring of SN 1987A at a distance of ~ 200 light days from the SN. The presence of highly ionized gas implied that the gas must have been ionized and heated by the radiation at shock break-out. Because of the finite light travel time across the ring, the observed total emission from the ring is a convolution of the emission at different epochs from the various part of the ring. Detailed modeling [55,56] shows that while the ionization of the ring occurs on the time scale of the soft X-ray burst, the gas recombines and cools on a time scale of years, explaining the persistence of the emission decades after the explosion. The observed line emission provides sensitive diagnostics of both the properties of the soft X-ray burst, and the density, temperature and abundances of the gas in the ring. In particular, the radiation temperature must have reached $\sim 10^6$ K, in good agreement with the most detailed recent modeling of the shock break-out [3]. Narrow emission lines are not unique to SN 1987A, but have also been observed for several other SNe, in particular several Type IIn SNe, such as SN 1995N [44] and SN 1998S [36].

The soft X-ray burst may also pre-accelerate the gas in front of the shock. In the conservative case that Thompson scattering dominates, the gas immediately in front of the shock will be accelerated to

$$V = 1.4 \times 10^3 \left(\frac{E}{10^{48} \text{ ergs}} \right) \left(\frac{V_s}{1 \times 10^4 \text{ km s}^{-1}} \right)^{-2} \left(\frac{t}{\text{days}} \right)^{-2} \text{ km s}^{-1}, \quad (17)$$

where E is the total radiative energy in the burst. Line absorption may further boost this [39]. If the gas is pre-accelerated, the line widths are expected to decrease with time. After about one expansion time ($\sim R_p/V$) the reverse and circumstellar shocks are fully developed, and the radiation from these will dominate the properties of the circumstellar gas. The fraction of this emission going inward is absorbed by the ejecta and there re-emitted as optical and UV radiation [37,38].

The X-ray emission from the shocks ionizes and heats both the circumstellar medium and the SN ejecta. Observationally, these components are distinguished easily by the different velocities. The circumstellar component is expected to have velocities typical of the progenitor winds, i.e., $\lesssim 1000$ km s $^{-1}$, while the ejecta have considerably higher velocities. The density is likely to

be of the order of the wind density $10^5 - 10^7 \text{ cm}^{-3}$, or higher if clumping is important. The ionizing X-ray flux depends strongly on how much of the flux from the reverse shock can penetrate the cool shell. The state of ionization in the circumstellar gas is characterized by the value of the ionization parameter, $\zeta = L_{\text{cs}}/(r^2 n) = 10^2 (L_{\text{cs}}/10^{40} \text{ erg s}^{-1})(r/10^{16} \text{ cm})^{-2}(n/10^6 \text{ cm}^{-3})^{-1}$ [50]. The comparatively high value of $\zeta \approx 10 - 10^3$ explains the presence of narrow coronal lines of [Fe V-XI] seen in objects like SN 1995N [44].

6.2 SN ejecta

The ingoing X-ray flux from the reverse shock ionizes the outer parts of the ejecta. The state of highest ionization therefore is close to the shock, with a gradually lower degree of ionization inwards. Unless clumping in the ejecta is important, the ejecta density is $\sim 10^6 - 10^8 \text{ cm}^{-3}$. In the left panel of figure 4 we show temperature and ionization structure of the ejecta, as well as the emissivity of the most important lines. The temperature close to the shock is $\sim 3 \times 10^4 \text{ K}$. Calculations show that most of the emission here is emitted as UV lines of highly ionized ions, like $\text{Ly}\alpha$, C III-IV, N III-V, and O III-VI. Inside the ionized shell there is an extended partially ionized zone, similar to that present in the broad emission line regions of AGN's. Most of the emission here comes from Balmer lines.

As we have already discussed, the outgoing flux from the reverse shock is to a large extent absorbed by the cool shell behind reverse shock and the contact discontinuity if radiative cooling has been important. The whole region behind the reverse shock is in approximate pressure balance, and the density of this gas is therefore be a factor $\sim 4T_{\text{rev}}/T_{\text{cool}} \approx 10^3 - 10^4$ higher than that of the ejecta. Because of the high density, the gas is only be partially ionized and the temperature only $(5 - 8) \times 10^3 \text{ K}$. Most of the emission comes out as Balmer lines, Mg II and Fe II lines (figure 4, right panel). The thickness of the emitting region is also very small, $\sim 3 \times 10^{12} \text{ cm}$. In one dimensional models, the velocity is marginally smaller than the highest ejecta velocities. Instabilities in the shock are, however, likely to erase this difference.

An important diagnostic of the emission from the cool shell and the ejecta is the $\text{H}\alpha$ line. This line arises as a result of recombination and collisional excitation. In [16], it is shown that $\sim 1\%$ of the reverse shock luminosity is emitted as $\text{H}\alpha$, fairly independent of density and other parameters. Observations of this line permit us to follow the total luminosity from the reverse shock, complementary to the X-ray observations. In SN 1993J, the $\text{H}\alpha$ line had the box-like shape that is expected for shocked, cooled ejecta [60,61]. The top of the line showed structure that varied with time; this could be related to hydrodynamic instabilities of the reverse shocked gas.

6.3 Interaction with dust

The winds from red supergiant stars are known to contain dust, so that infrared emission from radiatively heated dust and dust scattering of supernova light

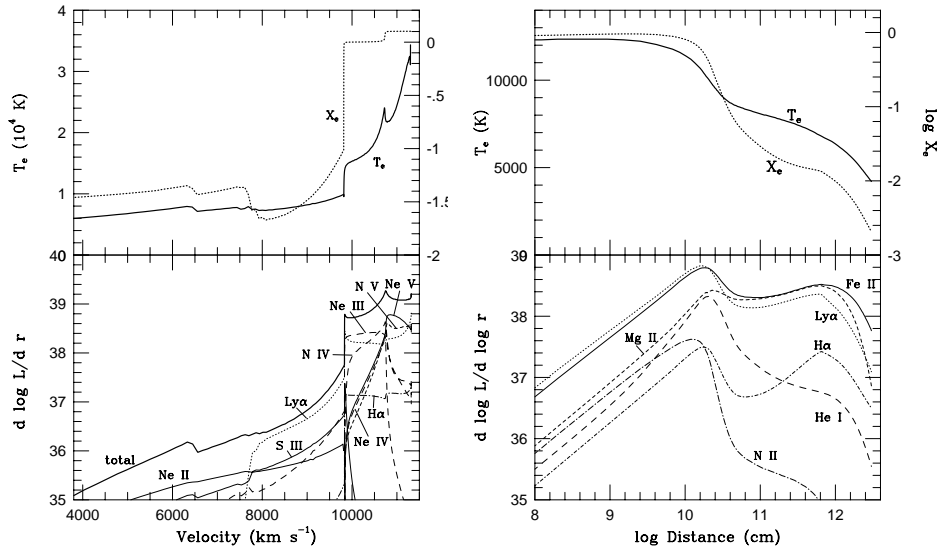


Fig. 4. Structure of the ejecta and cool shell ionized by the reverse shock at 500 days for parameters appropriate to SN 1993J ($\dot{M} = 5 \times 10^{-5} M_{\odot} \text{ yr}^{-1}$ for $u = 10 \text{ km s}^{-1}$). Upper panels show the temperature and ionization of the ejecta (left panels) and the cool shell (right panels), while the lower panels show the corresponding luminosities per unit distance. Note the different length scales in the two panels. The ejecta region has low density, high temperature and ionization, while the cool shell has a high density, is extremely thin, has a low temperature, and is only partially ionized.

might be expected. The dust temperature is determined by a balance between radiative heating and emission from the grain surface. If the supernova radiates like a blackbody of temperature T_{sn} and if the dust absorption efficiency varies as λ^{-q} , the grain temperature is $T_{\text{g}} = T_{\text{sn}} W^{1/(4+q)}$, where W is the dilution factor for the supernova radiation [28]. For $q = 1$, we have

$$T_{\text{g}} = 280 \left(\frac{T_{\text{sn}}}{5000 \text{ K}} \right)^{0.2} \left(\frac{L_{\text{sn}}}{10^{42} \text{ ergs s}^{-1}} \right)^{0.2} \left(\frac{r}{10^{18} \text{ cm}} \right)^{-0.4} \text{ K}, \quad (18)$$

where L_{sn} is the supernova luminosity.

Because typical evaporation temperatures for grain materials are in the range 1000 – 1500 K, the dust near the supernova is evaporated. The radius out to which dust is evaporated, r_v , is probably determined by the luminosity at the time of shock breakout, when L_{sn} can be $\gtrsim 10^{44} \text{ ergs s}^{-1}$. SN 1979C and SN 1980K were detected as infrared sources, and Dwek [28] estimates $r_v \approx 3 \times 10^{17} \text{ cm}$ in these cases. The infrared light curve can be calculated from T_{g} , taking into account light travel time effects. If the characteristic time that the supernova is bright is short compared to $2r_v/c$, there is a plateau phase until a time $2r_v/c$. The infrared flux then drops as t^{-2} for a highly extended wind and drops more rapidly

if the cutoff in the wind, r_w , is close to r_v . For SN 1979C and SN 1980K, Dwek [28] found $r_w \lesssim 10^{18}$ cm. The ratio of the infrared emitted energy to the total emitted energy gives an estimate of the optical depth through the dusty wind. The optical depths for SN 1979C and SN 1980K are ~ 0.3 and 0.03 , respectively, leading to minimum shell masses of $\sim 1 - 5 M_\odot$ and $\sim 0.1 - 0.4 M_\odot$ for the two supernovae [28]. The corresponding mass loss rates are consistent with those derived from radio observations [54]. Infrared emission that can be attributed to radiatively heated dust has recently been observed from SN 1998S [36]. Infrared dust echoes have the potential to give information on dust composition and distribution [29,32], but the observations do not yet exist to address these issues.

The dust grains that give an infrared echo can also give a scattered light echo [10]. The ratio between the total scattered light and the infrared light depends on the albedo of the dust. The light curve decreases with time before $2r_v/c$ in this case because of the strong forward scattering of typical grains. Chevalier [10] failed to find good evidence for scattered light echoes from SN 1979C and SN 1980K, although such echoes might have been observable. The implication may be that the dust grains have small albedos. The problem with detecting scattered light echoes is that any echo light may be dominated by light coming directly from the circumstellar interaction. Roscherr & Schaefer [68] examined the late emission from two Type IIn supernovae and determined that it was due to shock interaction. Because of the ability to spatially resolve the emission in SN 1987A, it has been possible to observe scattered light from the wind interaction nebula [23] and possibly a shell at the outer extent of the red supergiant wind [15].

7 Relativistic Particles

Unambiguous evidence for the presence of relativistic electrons comes from radio observations of SNe. A characteristic is the wavelength-dependent turn-on of the radio emission ([73]; chapter by Sramek), first seen at short wavelengths, and later at longer wavelengths. This behavior is interpreted as a result of decreasing absorption due to the expanding emitting region [9].

Depending on the magnetic field and the density of the circumstellar medium, the absorption may be produced either by free-free absorption in the surrounding thermal gas, or by synchrotron self-absorption by the same electrons that are responsible for the emission. The relativistic electrons are believed to be produced close to the interaction region, which provides an ideal environment for the acceleration of relativistic particles. The details of the acceleration and injection efficiency are still not well understood (see, e.g., [26] and references therein). Here we just parameterize the injection spectrum with the power law index p_1 and an efficiency, η , in terms of the postshock energy density. Without radiation or collisional losses the spectral index of the synchrotron emission will then be $\alpha = (p - 1)/2$, where flux $\propto \nu^{-\alpha}$. Diffusive acceleration predicts that $p_1 = 2$ in the test particle limit. If the particle acceleration is very efficient and nonlinear effects are important, the electron spectrum can be steeper (e.g., [31]).

For free-free absorption, the optical depth $\tau_{\text{ff}} = \int_{R_s}^{\infty} \kappa_{\text{ff}} n_e n_i dr$ from the radio emitting region close to the shock through the circumstellar medium decreases as the shock wave expands, explaining the radio turn-on. Assuming a fully ionized wind with constant mass loss rate and velocity, so that equation (2) applies, the free-free optical depth at wavelength λ is

$$\tau_{\text{ff}}(\lambda) \approx 7.1 \times 10^2 \lambda^2 \left(\frac{\dot{M}_{-5}}{u_{w1}} \right)^2 T_5^{-3/2} V_4^{-3} t_{\text{days}}^{-3} \quad (19)$$

where \dot{M}_{-5} is the mass loss rate in units of $10^{-5} M_{\odot} \text{ yr}^{-1}$, u_{w1} the wind velocity in units of 10 km s^{-1} , and T_5 the temperature of the circumstellar gas in 10^5 K . From the radio light curve, or spectrum, the epoch of $\tau_{\text{ff}} = 1$ can be estimated for a given wavelength, and from the line widths in the optical spectrum the maximum expansion velocity, V , can be obtained. Because the effects of the radiation from the supernova have to be estimated from models of the circumstellar medium, the temperature in the gas is uncertain. Calculations show that initially the radiation heats the gas to $T_e \approx 10^5 \text{ K}$ [54]. T_e then decreases with time, and after a year $T_e \approx (1.5 - 3) \times 10^4 \text{ K}$. In addition, the medium may recombine, which further decreases the free-free absorption. From $t[\tau(\lambda)_{\text{ff}} = 1]$ the ratio \dot{M}/u_w can be calculated. Because $\dot{M}/u_w \propto T_e^{3/4} x_e^{-1}$, errors in T_e and x_e may lead to large errors in \dot{M} . If the medium is clumpy, equation (19) may lead to an overestimate of \dot{M}/u_w .

Under special circumstances (see below), synchrotron self-absorption (SSA) by the same relativistic electrons emitting the synchrotron radiation may be important [70,12,40]. The emissivity of the synchrotron plasma is given by $j(\lambda) = \text{const. } \lambda^{\alpha} B^{1+\alpha} N_{\text{rel}}$ [53], while the optical depth to self-absorption is given by

$$\tau_s = \text{const. } \lambda^{(5/2)+\alpha} B^{(3/2)+\alpha} N_{\text{rel}} . \quad (20)$$

Here N_{rel} is the column density of relativistic electrons and B the magnetic field. The flux from a disk with radius R_s of relativistic electrons is, including the effect of SSA, given by

$$F_{\nu}(\lambda) \propto R_s^2 S(\lambda) [1 - e^{-\tau_s(\lambda)}], \quad (21)$$

where $S(\lambda) = j(\lambda)/\kappa(\lambda) = \text{const. } \lambda^{-5/2} B^{-1/2}$ is the source function. In the optically thick limit we therefore have $F_{\nu}(\lambda) \approx \text{const. } R_s^2 \lambda^{-5/2} B^{-1/2}$, independent of N_{rel} . A fit of this part of the spectrum therefore gives the quantity $R_s^2 B^{-1/2}$. The break of the spectrum determines the wavelength of optical depth unity, $\lambda(\tau_s = 1)$. Equation (20) therefore gives a second condition on $B^{3/2+\alpha} N_{\text{rel}}$. If $R_s(t)$ is known in some independent way, one can determine both the magnetic field and the column density of relativistic electrons, independent of assumptions about equipartition, etc. In some cases, most notably for SN 1993J, the shock radius, R_s , can be determined directly from VLBI observations. If this is not possible, an alternative is from observations of the maximum ejecta velocity seen in, e.g., the $\text{H}\alpha$ line, which should reflect the velocity of the gas close

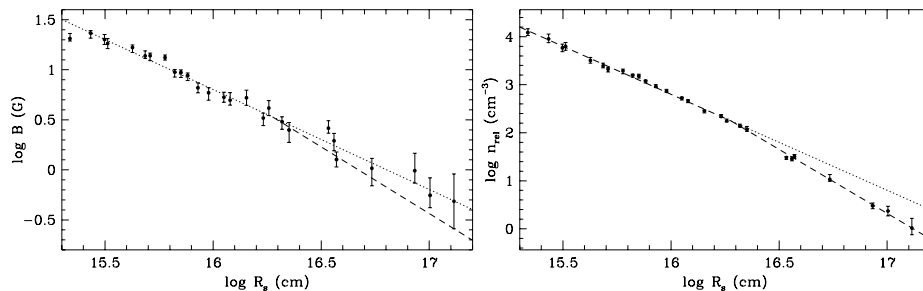


Fig. 5. Magnetic field (left) and density of relativistic electrons (right) as a function of the shock radius for SN 1993J. The dashed lines show the expected evolution if the magnetic energy density and relativistic particle density scale with the thermal energy density, $B^2/8\pi \propto \rho V_s^2 \propto n_{\text{rel}} \propto t^{-2}$, while the dotted lines show the case when $B \propto r^{-1}$ and $n_{\text{rel}} \propto r^{-2}$ [40].

to the shock. Because the SN expands homologously, $R_s = V_{\text{max}}t$. A fit of the spectrum at a given epoch can therefore yield both B and N_{rel} independently. From observations at several epochs the evolution of these quantities can then be determined.

Although the injected electron spectrum from the shock is likely to be a power law with $p_i \approx 2$ ($\alpha \approx 0.5$), the integrated electron spectrum is affected by various loss processes. Most important, the synchrotron cooling time scale of an electron with Lorentz factor γ is $t_{\text{syn}} \approx 9 \times 10^3 \gamma^{-1} B^{-2}$ days. This especially affects the high energy electrons, steepening the index of the electron spectrum by one unit, $p = p_i + 1 \approx 3$ ($\alpha \approx 1$). Inverse Compton losses have a similar effect. At low energy, Coulomb losses may be important, causing the electron spectrum to flatten.

The best radio observations of any SN were obtained for SN 1993J. This SN was observed from the very beginning until late epochs with the VLA at wavelengths between 1.3 – 90 cm [77], producing a set of beautiful light curves (see also Chapter by Sramek). In addition, the SN was observed with VLBI [57,58,2], resulting in an impressive sequence of images in which the radio emitting plasma could be directly observed. These images showed a remarkable degree of symmetry and clearly resolved the shell of emitting electrons. The evolution of the radius of the radio emitting shell could be well fitted by $R_s \propto t^{0.86}$, implying a deceleration of the shock front.

From a fit of the observed spectra for the different epochs the magnetic field and number of relativistic electrons could be determined for each epoch, as described above [40]. In figure 5 we show the evolution of B and particle density n_{rel} , plotted as a function of the shock radius. The most remarkable thing is the smooth evolution of these quantities, showing that $B \approx 6.4(R_s/10^{16} \text{ cm})^{-1}$ G, and $n_{\text{rel}} \propto \rho V^2 \propto t^{-2}$, the thermal energy density behind the shock. The magnetic field is close to equipartition, $B^2/8\pi \approx 0.14 \rho V_s^2$, much higher than expected if the circumstellar magnetic field, of the order of a few mG, was just

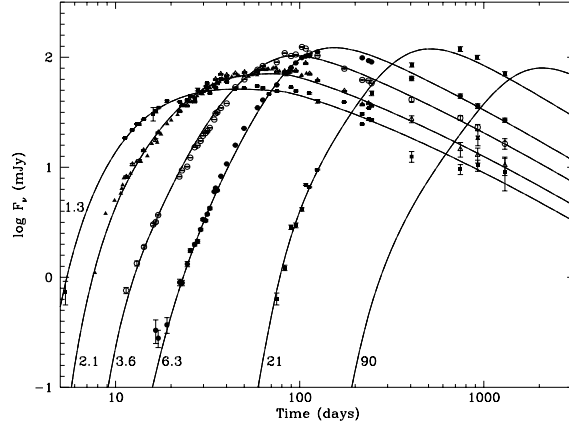


Fig. 6. Observed [77] and model radio light curves of SN 1993J [40].

compressed, and strongly argues for field amplification, similar to what has been seen in simulations [48]. Contrary to earlier, simplified models for SN 1993J based on free-free absorption only [41,77], the circumstellar density was consistent with $\rho \propto r^{-2}$.

In figure 6, we show the excellent fit of the resulting light curves. The high values of B implied that synchrotron cooling was important throughout most of the evolution for the electrons responsible for the cm emission, and also for the 21 cm emission before ~ 100 days. At early epochs, Coulomb losses were important for the low energy electrons. The injected electron spectrum was best fitted with $p_i = 2.1$.

The form of the light curves can be understood if, for simplicity, we *assume* equipartition, so that $B^2/8\pi = \eta\rho V_s^2$. With $\rho \propto (\dot{M}/u) R_s^{-2}$ and $V_s \propto R_s/t$, we find that $B \propto (\dot{M}/u)^{1/2} t^{-1}$. The optically thick part is therefore given by

$$F_\nu(\lambda) \propto R_s^2 \lambda^{-5/2} B^{-1/2} \propto (\dot{M}/u)^{-1/4} \lambda^{-5/2} t^{(5n-14)/2(n-2)}, \quad (22)$$

since $R_s \propto t^{(n-3)/(n-2)}$. For large n , we get $F_\nu(\lambda) \propto t^{5/2}$. An additional curvature of the spectrum is produced by free-free absorption in the wind, although this only affects the spectrum at early epochs.

In the optically thin limit, $F_\nu(\lambda) \propto R_s^2 j(\lambda) \propto R_s^2 \lambda^\alpha B^{1+\alpha} N_{\text{rel}}$. If losses are unimportant, $N_{\text{rel,tot}} = 4\pi R_s^2 N_{\text{rel}}$, the total number of relativistic electron, may either be assumed to be proportional to the total mass, if a fixed fraction of the shocked electrons are accelerated, or be proportional to the swept up thermal energy. In the first case, $N_{\text{rel,tot}} \propto \dot{M} R_s / u_w$, while in the second $N_{\text{rel,tot}} \propto \dot{M} R_s V_s^2 / u_w$, so that in general $N_{\text{rel,tot}} \propto \dot{M} R_s V_s^{2\epsilon} / u_w$, where $\epsilon = 0$ or 1 in these two cases. Therefore, $F_\nu(\lambda) \propto \dot{M}/u R_s V_s^{2\epsilon} \lambda^\alpha B^{1+\alpha}$. If the B-field is in equipartition, as above, and using $V = (n-3)/(n-2) R_s/t \propto t^{-1/(n-2)}$ we find

$$F_\nu(\lambda) \propto (\dot{M}/u_w)^{(3+\alpha)/2} \lambda^\alpha t^{-\alpha-(1+2\epsilon)/(n-2)}. \quad (23)$$

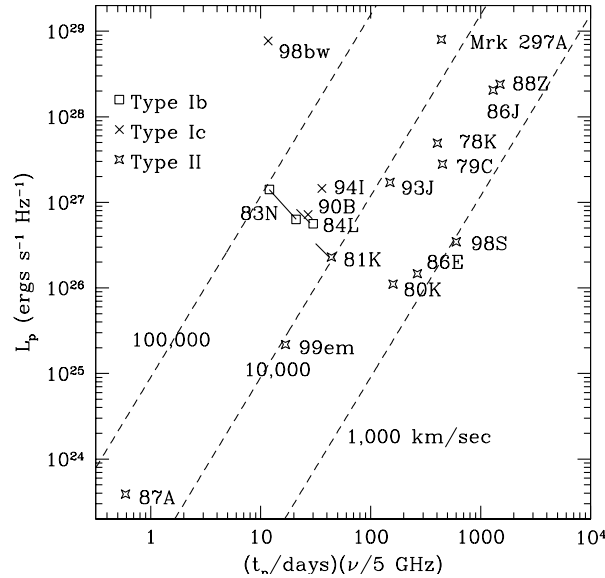


Fig. 7. Peak luminosity and corresponding epoch for the well-observed radio SNe. The dashed lines give curves of constant expansion velocity, *assuming* SSA (see [12]).

If synchrotron cooling is important, a similar type of expression can be derived [40]. The main thing to note is, however, that the optically thin emission is expected to be proportional to the mass loss rate, \dot{M}/u_w , and that the decline rate depends on whether the number of relativistic particles scale with the number density or the thermal energy of the shocked gas, as well as spectral index. Observations of the decline rate can therefore test these possibilities.

Although a self-consistent model can be developed for SN 1993J and other radio supernovae, the modeling of SN 1986J and related objects has been unclear. Weiler, Panagia, & Sramek [79] proposed a model for SN 1986J in which thermal absorbing material is mixed in with the nonthermal emission; one possibility for this is a very irregular shocked emission region. The absorption is described in a parameterized way and is not related to a quantitative supernova model. Chugai & Belous [20] propose a model in which the absorption is by clumps. The narrow line optical emission implies the presence of clumps, but they are different from those required for the radio absorption. The possible presence of clumps and irregularities introduces uncertainties into models for the radio emission, although rough estimates of the circumstellar density can still be obtained.

The relative importance of SSA and free-free absorption depends on a number of parameters and we refer to [12,40] for a more detailed discussion. The most important of these are the mass loss rate, \dot{M}/u_w , the shock velocity, V_s , and the circumstellar temperature, T_e . In general, a high shock velocity and a high

circumstellar temperature favor SSA, while a high mass loss rate favors free-free absorption.

Assuming SSA, an interesting expression for the velocity of the shock can be derived which can be tested against the observations. If we assume equipartition, $N_{\text{rel}} \propto \rho V_s^2 R_s$ and $B^2/8\pi \propto \rho V_s^2$ we have $N_{\text{rel}} \propto B^2 R_s$. Using this in equation (20) we get $\tau_s = \text{const } \lambda^{5/2+\alpha} B^{7/2+\alpha} R_s$. The peak in the light curve is given by $\tau_s \approx 1$. If we approximate the flux at this point by the optically thick expression equation (22) and solve for B we get $B \propto F_\nu(\lambda)^{-2} R_s^4 \lambda^{-5}$. Inserting this expression in the condition $\tau_s \approx 1$, we find $R_s^{15+4\alpha} F_\nu(\lambda)^{-7-2\alpha} \lambda^{-15-4\alpha} \approx \text{const}$. With $V_s = (n-3)/(n-2)R_s/t$ we finally have

$$V_s \approx \text{const } F_\nu(\lambda)^{(7+2\alpha)/(15+4\alpha)} \lambda t^{-1} \quad (24)$$

where all parameters refer to their values at the peak of the light curve. Using this expression, we can plot lines of constant shock velocity into a diagram with peak radio luminosity versus time of peak flux, *assuming* that SSA dominates (figure 7). The positions of the lines depend only weakly on the equipartition assumption. Each SN can now be placed in this diagram to give a predicted shock velocity. If this is lower than the observed value (as measured by VLBI or from line profiles) SSA gives a too low flux and should therefore be relatively unimportant and free-free absorption instead dominate. In figure 7 we show an updated version of the figure in [12]. The most interesting point is that most Type Ib/Ic SNe, SN 1983N, SN 1994I and SN 1998bw, fall into the high velocity category, while Type IIL SNe, like SN 1979C and SN 1980K, as well as the Type IIn's SN 1978K, SN 1988Z, SN 1998S fall in the free-free group. SN 1987A is clearly special with its low mass loss rate, but is most likely dominated by SSA [74,70,14]. Mrk 297A is an apparent radio supernova in the clumpy, irregular galaxy Mrk 297 [82]; its supernova type is not known.

8 Discussion and conclusions

Circumstellar interaction of supernovae gives an important window on the nature of stars that explode and their evolution leading up to the explosion. Mass loss rates for the red supergiant progenitors of Type II supernovae range from $\sim 2 \times 10^{-6} M_\odot \text{ yr}^{-1}$ for SN 1999em [66] to $\gtrsim 2 \times 10^{-4} M_\odot \text{ yr}^{-1}$ for SN 1979C and SN 1986J [54]. Evidence for CNO processing has been found in a number of supernovae, including SN 1979C [42], SN 1987A [43] and SN 1995N [44]. In some cases, the reverse shock appears to be moving into gas that is H poor and O rich, e.g., SN 1995N [44]; this relates to the total amount of mass loss before the supernova. The complex circumstellar environment of SN 1987A has become clear because of its proximity (see Chapter by McCray). For more distant supernovae, studies of polarization and spectral line profiles can reveal asymmetries, as in SN 1998S [52].

The evidence on circumstellar interaction is especially useful when it can be combined with information from other aspects of the supernovae, such as their light curves and stellar environments. For example, from the pre-supernova

stellar environment of SN 1999em, Smartt et al. [71] deduced an initial mass of $12 \pm 1 M_{\odot}$. The supernova was of the plateau type, implying that hydrogen envelope was largely intact at the time of the supernova. This is consistent with the relatively low rate of mass loss deduced for the supernova progenitor [66].

In addition to information on the evolution of massive stars and their explosions, circumstellar interaction provides an excellent laboratory for the study of shock wave physics. Compared to older supernova remnants, the shock velocities are higher and the time evolution gives an additional dimension for study, although there is little spatial information in most cases. VLBI observations can, however, in this respect be extremely valuable, as demonstrated by SN 1993J. An object where both the spatial and time dimensions are accessible is SN 1987A, which has turned out to be an excellent source for the study of shock waves (see Chapter by McCray).

We are grateful to John Blondin for providing Figure 2 and to Peter Lundqvist for comments on the manuscript. This work was supported in part by NASA grant NAG5-8232 and by the Swedish Research Council.

References

1. W.D. Arnett: ApJ **331**, 377 (1988)
2. N. Bartel, et al.: Science **287**, 112 (2000)
3. S. Blinnikov, P. Lundqvist, O. Bartunov, K. Nomoto, K. Iwamoto: ApJ **532**, 1132 (2000)
4. J.M. Blondin, P. Lundqvist, R.A. Chevalier: ApJ **472**, 257 (1996)
5. D. Branch, M. Livio, L.R. Yungelson, F.R. Boffi, E. Baron: PASP **107**, 1019 (1995)
6. C.J. Burrows, et al.: ApJ **452**, 680 (1995)
7. R.A. Chevalier: ApJ **207**, 872 (1976)
8. R.A. Chevalier: ApJ **258**, 790 (1982)
9. R.A. Chevalier: ApJ **259**, 302 (1982)
10. R.A. Chevalier: ApJ **308**, 225 (1986)
11. R.A. Chevalier: In *Supernovae*, ed. by A.G. Petschek, (Springer, Berlin 1990) p. 91
12. R.A. Chevalier: ApJ **499**, 810 (1998)
13. R.A. Chevalier, J.M. Blondin: ApJ **444**, 312 (1995)
14. R.A. Chevalier, V.V. Dwarkadas: ApJ **452**, L45 (1995)
15. R.A. Chevalier, R.T. Emmering: ApJ **342**, L75 (1989)
16. R.A. Chevalier, C. Fransson: ApJ **420**, 268 (1994)
17. R.A. Chevalier, N. Soker: ApJ **341**, 867 (1989)
18. R.A. Chevalier, J.M. Blondin, R.T. Emmering: ApJ **392**, 118 (1992)
19. N.N. Chugai: ApJ **414**, L101 (1993)
20. N.N. Chugai, M.L. Belous: Astr. Rep. **43**, 89 (1999)
21. N.N. Chugai, I.J. Danziger: MNRAS **268**, 173 (1994)
22. N.N. Chugai, I.J. Danziger, M. Della Valle: MNRAS **276**, 530 (1995)
23. A.P.S. Crotts, W.E. Kunkel, S.R. Heathcote: ApJ **438**, 724 (1995)
24. R.J. Cumming, P. Lundqvist, L.J. Smith, M. Pettini, and D.L. King: MNRAS **283**, 1355 (1996)
25. W.C. Danchi, et al.: AJ **107**, 1469 (1994)
26. B.T. Draine, C.F. McKee: ARA&A **31**, 373 (1993)
27. V.V. Dwarkadas, R.A. Chevalier: ApJ **497**, 807 (1998)

28. E. Dwek: ApJ **274**, 175 (1983)
29. E. Dwek: ApJ **297**, 719 (1985)
30. E. Dwek: ApJ **322**, 812 (1987)
31. D.C. Ellison, S.P. Reynolds: ApJ **382**, 242 (1991)
32. R.T. Emmering, R.A. Chevalier: AJ **95**, 152 (1988)
33. L. Ensman, A. Burrows: ApJ **393**, 742 (1992)
34. S.W. Falk: ApJ **226**, L133 (1978)
35. S.W. Falk, W.D. Arnett: ApJ **180**, L65 (1973)
36. A. Fassia, et al.: MNRAS **318**, 1093 (2000)
37. C. Fransson: A&A **111**, 140 (1982)
38. C. Fransson: A&A **133**, 264 (1984)
39. C. Fransson: in *Highlights of Astronomy* **7**, 611 (1986)
40. C. Fransson, C.-I. Björnsson: ApJ **509**, 861 (1998)
41. C. Fransson, P. Lundqvist, R.A. Chevalier: ApJ **461**, 993 (1996)
42. C. Fransson, P. Benvenuti, W. Wamsteker, C. Gordon, K. Hempe, D. Reimers, G.G.C. Palumbo, N. Panagia: A&A **132**, 1 (1984)
43. C. Fransson, A. Cassatella, R. Gilmozzi, R.P. Kirshner, N. Panagia, G. Sonneborn, W. Wamsteker: ApJ **336**, 429 (1989)
44. C. Fransson, et al.: ApJ, submitted (astro-ph/0108149) (2001)
45. G. García-Segura, N. Langer, M.-M. MacLow: A&A **316**, 133 (1996)
46. J.C. Houck, J.N. Bregman, R.A. Chevalier, K. Tomisaka: ApJ **493**, 431 (1998)
47. P. Jakobsen, et al.: ApJ **369**, L63 (1991)
48. B. Jun, M.L. Norman: ApJ **472**, 245 (1996)
49. B. Jun, T.W. Jones, M.L. Norman: ApJ **468**, L59 (1996)
50. T.R. Kallman, R. McCray: ApJS **50**, 263 (1982)
51. R.I. Klein, R.A. Chevalier: ApJ **223**, L109 (1978)
52. D.C. Leonard, A.V. Filippenko, A.J. Barth, T. Matheson: ApJ **536**, 239 (2000)
53. M.S. Longair: *High Energy Astrophysics*, Cambridge University Press (1992)
54. P. Lundqvist, C. Fransson: A&A **192**, 221 (1988)
55. P. Lundqvist, C. Fransson: ApJ **380**, 575 (1991)
56. P. Lundqvist, C. Fransson: ApJ **464**, 924 (1996)
57. J.M. Marcaide, et al.: Science **270**, 1475 (1995)
58. J.M. Marcaide, et al.: ApJ **486**, L31 (1997)
59. E. Marietta, A. Burrows, B. Fryxell: ApJ Supp **128**, 615 (2000)
60. T. Matheson, et al.: AJ **120**, 1487 (2000)
61. T. Matheson, A.V. Filippenko, L.C. Ho, A.J. Barth, D.C. Leonard: AJ **120**, 1499 (2000)
62. C.D. Matzner, C.F. McKee: ApJ **510**, 379 (1999)
63. A.R. McDonald, T.W.B. Muxlow, A. Pedlar, M.A. Garrett, K.A. Willis, S.T. Gar-
rington, P. Diamond, P.N. Wilkinson: MNRAS **322**, 100 (2001)
64. D.K. Nadyozhin: Ap&SS **112**, 225 (1985)
65. N. Panagia, et al.: MNRAS **192**, 861 (1980)
66. D. Pooley, et al.: ApJ, submitted (astro-ph/0103196) (2001)
67. A.M.S. Richards, J.A. Yates, R.J. Cohen: MNRAS **299**, 319 (1998)
68. B. Roscherr, B.E. Schaefer: ApJ **532**, 415 (2000)
69. N. Smith, R. M. Humphreys, K. Davidson, R.D. Gehrz, M.T. Schuster, J. Krautter:
AJ **121**, 1111 (2001)
70. V.I. Slysh: Sov. Astr. Lett. **16**, 339 (1990)
71. S.J. Smartt, G.F. Gilmore, C.A. Tout, S.T. Hodgkin: ApJ, submitted (astro-
ph/0107499) (2001)

72. G. Sonneborn, C. Fransson, P. Lundqvist, A. Cassatella, R. Gilmozzi, R.P. Kirshner, N. Panagia, W. Wamsteker: *ApJ* **477**, 848 (1997)
73. R.A. Sramek, K.W. Weiler: In *Supernovae*, ed. by A.G. Petschek, (Springer, Berlin 1990) p. 76
74. M. Storey, R.N. Manchester: *Nature* **329**, 421 (1987)
75. P.G. Tuthill, C.A. Haniff, J.E. Baldwin: *MNRAS* **285**, 529 (1997)
76. H. Uitenbroek, A.K. Dupree, R.L. Gilliland: *AJ* **116**, 2501 (1998)
77. S.D. van Dyk, K.W. Weiler, R.A. Sramek, M.P. Rupen, N. Panagia: *ApJ* **432**, L115 (1994)
78. L. Wang: *A&A* **246**, L69 (1995)
79. K.W. Weiler, N. Panagia, R.A. Sramek: *ApJ* **364**, 611 (1990)
80. A.J. Willis: In *Wolf-Rayet Stars and Interrelations with Other Massive Stars in Galaxies*. ed. by K.A. van der Hucht & B. Hidayat, (Kluwer, Dordrecht 1991) p. 265
81. M. Wittkowski, N. Langer, G. Weigelt: *A&A* **340**, L39 (1998)
82. Q.F. Yin: *ApJ* **420**, 152 (1994)